'Unconventional' Coordination Chemistry by Metal Chelating Fragments in a Metalloprotein Active Site

David P. Martin,[†] Patrick G. Blachly,[†] Amy R. Marts,[‡] Tessa M. Woodruff,[‡] César A. F. de Oliveira,[∥] J. Andrew McCammon,[†,§,∥] David L. Tierney,*[,‡] and Seth M. Cohen*[,†]

[†]Department of Chemistry and Biochemistry, [§]Pharmacology, and [∥]Howard Hughes Medical Institute, University of California, San Diego, La Jolla, California 92093, United States

[‡]Department of Chemistry and Biochemistry, Miami University, Oxford, Ohio 45056, United States

S *Supporting Information*

ABSTRACT: The binding of three closely related chelators: 5-hydroxy-2-methyl-4*H*-pyran-4-thione (allothiomaltol, ATM), 3-hydroxy-2-methyl-4*H*-pyran-4-thione (thiomaltol, TM), and 3-hydroxy-4*H*-pyran-4-thione (thiopyromeconic acid, TPMA) to the active site of human carbonic anhydrase II (hCAII) has been investigated. Two of these ligands display a monodentate mode of coordination to the active site Zn^{2+} ion in hCAII that is not recapitulated in model complexes of the enzyme active site. This unprecedented binding mode in the hCAII-thiomaltol complex has been characterized by both X-ray crystallography and X-ray spectroscopy. In addition, the steric restrictions of the active site force the ligands into a 'flattened' mode of coordination compared with inorganic model complexes. This change in geometry has been shown by density functional computations to significantly decrease the strength of the metal−ligand binding. Collectively, these data demonstrate that the mode of binding by small metal-binding groups can be significantly influenced by the protein active site. Diminishing the strength of the metal−ligand bond results in unconventional modes of metal coordination not found in typical coordination compounds or even carefully engineered active site models, and understanding these effects is critical to the rational design of inhibitors that target clinically relevant metalloproteins.
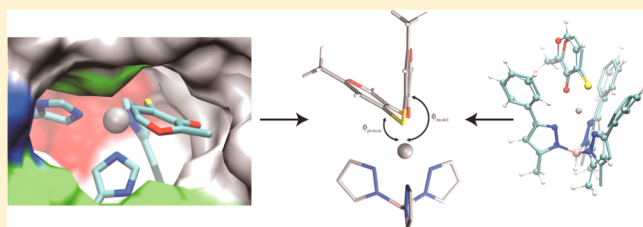
INTRODUCTION

Metalloproteins represent a significant fraction of the human proteome, and many represent important therapeutic targets.[1] With respect to the latter, a large number of metalloprotein inhibitors have been developed, with clinically approved inhibitors available for the Zn^{2+}-dependent histone deacetylases (HDACs), angiotension converting enzyme (ACE), and carbonic anhydrase (CA), among others.[2,3] In the majority of these examples, the small molecule inhibitors possess functional groups that bind to the active site metal ion of the enzyme;[4] a relatively small selection of such groups, including carboxylates, phosphates, and hydroxamic acids, are commonly employed as the metal-binding groups (MBGs) of choice.[5] Recently, a number of efforts have focused on the development of alternative MBGs to these commonly employed groups,[6] and indeed some newer metalloprotein inhibitors, such as raltegravir and dolutegravir that target HIV integrase (HIV1 IN, Mg^{2+}-dependent), employ more sophisticated heterocyclic MBGs.[7−9] These next-generation MBGs have the potential to improve the potency, selectivity, and pharmacokinetics of metalloprotein-targeted therapeutics.

As is the case with other forms of inhibitor and drug development, the use of structure-aided design can be invaluable to metalloprotein inhibitor design. In previous efforts, inorganic model compounds have been utilized to predict the binding of ligands to metalloprotein active

sites.[10−16] Although this approach can be effective, the constrained interactions and nuances of a metalloprotein active site cannot be readily recapitulated in such model scaffolds. Several examples of metalloprotein active sites influencing metal−ligand coordination have been reported. Specifically, changes in coordination caused by interactions with the surrounding active site have been observed with inhibitors of carboxypeptidase A based on the *N*-hydroxyurea MBG as well as inhibitors of thermolysin that utilize an α-mercaptoketone MBG.[17,18] In both cases, the changes in metal coordination are the result of large aromatic groups on the inhibitor being positioned to form significant interactions with hydrophobic regions of the active site, and the coordination involved is relatively weak.

Despite being a poor MBG for most metalloproteins, the arylsulfonamide MBG (acetazolamide, Figure 1) dominates the design of inhibitors of carbonic anhydrases (CAs).[19] CA inhibitors are used in the treatment of glaucoma, epilepsy, and altitude sickness.[3] The potency of sulfonamides for CAs is attributed largely to optimized protein−MBG interactions upon binding the catalytic Zn^{2+} ion; the metal-bound amine and one of the sulfonamide oxygen atoms both form strong hydrogen bonds with nearby amino acid residues. In addition, the second
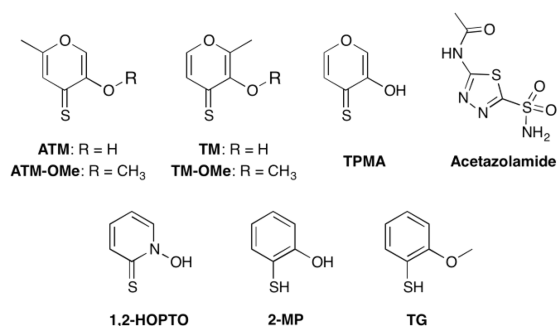
Figure 1. Structures of ATM, TM, TPMA, and several previously reported hCAII inhibitors: acetazolamide, based on the arylsulfonamide MBG, 1,2-HOPTO, 2-mercaptophenol (2-MP) and its methylated analog thioguaiacol (TG).

sulfonamide oxygen and the aromatic ring are positioned to occupy the substrate binding pocket of the enzyme active site.

In order to elucidate the binding of MBGs to metalloproteins as compared to model compounds, this report describes the binding of a series of closely related heterocyclic chelators to the active site of human carbonic anhydrase II (hCAII) and an inorganic model complex. Because it has many characteristics that make it a suitable model system including its rigid structure and ease of crystallization, hCAII has been widely used to examine protein−ligand interactions.[20,21] In the present study, the MBGs of interest are O,S-donor ligands based on a hydroxythiopyrone scaffold. Specifically, the three ligands, 5-hydroxy-2-methyl-4H-pyran-4-thione (allothiomaltol, ATM), 3-hydroxy-2-methyl-4H-pyran-4-thione (thiomaltol, TM), and 3-hydroxy-4H-pyran-4-thione (thiopyromeconic acid, TPMA), which differ only by the presence and/or position of a single methyl group, are examined (Figure 1). In model complexes based on a tris(pyrazolyl)borate (Tp) platform, these chelators bind in an identical, bidentate manner.[15] In contrast, in the active site of hCAII these chelators display a variety of coordination modes with the active site Zn^{2+} ion, including an unprecedented monodentate mode of binding by thiomaltol. The results not only show the utility but also the limitations of bioinorganic modeling while highlighting the subtle influence of active site structure on metal−ligand bonding. Such subtle effects on coordination chemistry are not readily predicted by current paradigms in bioinorganic chemistry and, consequently, are not implemented in standard drug design efforts directed at metalloproteins. Taken together, the findings presented here demonstrate that metal coordination by an exogenous ligand in a metalloprotein active site is strongly influenced by the protein active site. Existing drug design protocols for metalloproteins will need to be adapted to account for these perturbations.

EXPERIMENTAL SECTION

Synthesis. MBGs and $Tp^{Ph,Me}Zn(ATM)$ ($Tp^{Ph,Me}$ = hydrotris(5,3-methylphenylpyrazolyl)borate) were synthesized using modified reported procedures.[15,22] Details can be found in the Supporting Information.

hCAII Activity Assay. As previously reported,[23] hCAII was expressed and purified, and a detailed procedure can be found in the Supporting Information. Assays were performed in 50 mM HEPES pH 8.0 containing Na_2SO_4 to an ionic strength of 100 mM. Enzyme (100 nM final concentration) was incubated with varying concentrations of inhibitor for 10 min at room temperature before the addition of substrate (p-nitrophenyl acetate, final concentration between 50 μM and 10 mM). The reaction was monitored by the increase in absorbance at 405 nm. Initial reaction rates vs substrate

concentration were plotted for three concentrations of inhibitor, and the curves simultaneously fit for K_i using GraphPad Prism. Representative examples of curve fitting are included in the Supporting Information.

hCAII Crystallization. Crystals of hCAII were obtained by the sitting-drop or hanging-drop vapor diffusion method. The protein solution consisted of 20 mg/mL hCAII and 1 mM p-chloromercuribenzoic acid in 50 mM Tris-SO_4, pH 8.0. The precipitant solution contained 2.7−3.0 M $(NH_4)_2SO_4$ in 50 mM Tris-SO_4 pH 8.15. Drops consisted of 3 μL of protein solution plus 2.5−4.0 μL of precipitant solution and were equilibrated at 18 °C against 750 μL of precipitant solution. Crystals roughly 0.3 × 0.3 × 0.3 mm in size appeared after 2 days to 3 weeks. Once formed, crystals were transferred to 15 μL of soak solutions containing inhibitor (at saturation, ~1 mM), 1.5 M sodium citrate, 50 mM HEPES pH 8.15, 5% glycerol, and 2−5% DMSO. Crystals were taken directly from the soak solutions for data collection. Due to potential interference from the high concentration of DMSO necessary for ligand solubility, cocrystallization of the ligands with hCAII was not attempted.

Crystal Structure Determination. X-ray diffraction studies on hCAII crystals were carried out at 100 K with a Bruker D8 Smart 6000 CCD detector and utilizing Cu Kα radiation (λ = 1.5478 Å) from a Bruker-Nonius FR-591 rotating anode generator. The data were integrated and scaled using the Bruker APEX software suite. All crystals belonged to the monoclinic space group $P2_1$. The data were phased by molecular replacement using a previously reported hCAII structure (PDB 3KS3)[24] with water molecules removed. Models were built by alternating refinement using REFMAC5[25] and manual visualization and model building in Coot.[26] Ligand topologies were generated using the PRODRG server.[27] The structures have been deposited in the Protein Data Bank (PDB IDs 4MLX and 4MLT for ATM and TM, respectively). Mercury salts are commonly used in hCAII crystallization to increase crystal quality and size. Both structures contain p-mercuribenzoic acid bound to Cys206. Complete data collection details and refinement statistics for the $Tp^{Ph,Me}Zn$-(ATM) and hCAII crystal structures can be found in the Supporting Information.

X-ray Absorption Spectroscopy. Samples for XAS (~2 mM in protein) were prepared from lyophilized CA (Sigma Aldrich), dissolved in 50 mM phosphate buffer (pH 7.5) that was dialyzed overnight against the same buffer to remove salts and adventitious metals. MBG complexes were prepared by addition of a buffered solution of the MBG to the hCAII solution to a final concentration of 6 mM (3-fold molar excess). All samples contained 20% (v/v) glycerol as a glassing agent and were loaded in Lucite cuvettes with 6 μm polypropylene windows before being frozen rapidly in liquid nitrogen. X-ray absorption spectra were measured at the National Synchrotron Light Source (NSLS), beamline X3B, with a Si (111) double-crystal monochromator; harmonic rejection was accomplished using a Ni focusing mirror. Fluorescence excitation spectra for all samples were measured with a 31-element solid-state Ge detector array. Samples were held at ~15 K in a Displex cryostat. Detailed data collection and reduction procedures can be found in the Supporting Information.

Density Functional Computations. All geometry optimizations were performed using the Gaussian 09 suite of programs,[28] utilizing Becke's three-parameter hybrid method with the Lee, Yang, and Parr correlation functional (B3LYP)[29−32] with the 6-311+G(d,p) basis set and CPCM solvation (ε = 10).[33−35] The B3LYP functional has previously been used to successfully recapitulate geometric parameters of model active sites for Zn^{2+} metalloproteins[36] as well as free energies of water-chloride exchange in zinc chloride complexes.[37] Additional details and explanations can be found in the Supporting Information. Linear transit calculations were performed with the phenyl groups of $Tp^{Ph,Me}Zn$ omitted; this modified system is referred to as TpZn.

RESULTS

hCAII Inhibition. Previously reported data from screening a library of MBGs against hCAII revealed TM and TPMA as moderately potent fragments.[3] Determination of K_i values for

5401

dx.doi.org/10.1021/ja500616m | J. Am. Chem. Soc. 2014, 136, 5400−5406

ATM, TM, and TPMA reveals inhibition constants consistent with these early reports (Table 1). The effect of the inhibitors

Table 1. K_i Values (mM) of Compounds Against hCAII

compound	K_i	compound	K_i
ATM	0.65 ± 0.06	ATM-OMe	6.9 ± 1.0
THM	1.4 ± 0.2	THM-OMe	>50
TPMA	1.1 ± 0.2		

on the K_m curve of hCAII-catalyzed hydrolysis of p-nitrophenyl acetate is consistent with competitive inhibition (Figure S1). While TM and TPMA have similar K_i values (1.4 ± 0.2 and 1.1 ± 0.2 mM, respectively), ATM is roughly 2-fold more potent (0.65 ± 0.06 mM). When the hydroxyl group of ATM is methylated (ATM-OMe, Figure 1), the molecule drops ∼10-fold (K_i = 6.9 ± 1.0 mM) in potency. In contrast, methylation of TM (i.e., TM-OMe) results in a complete loss of inhibitory activity against hCAII ($K_i \gg 50$ mM).

Binding Mode Analysis. In order to explain the variation in inhibitory activity for this series of molecules, the X-ray crystal structures of ATM and TM bound to $Tp^{Ph,Me}Zn$ model compounds and the hCAII active site were examined. The crystal structure of TM bound to this model complex has been previously reported,[15,16] and ATM shows a very similar binding mode to the Zn^{2+} ion. The ligands bind in a bidentate fashion, resulting in trigonal bipyramidal geometry around the Zn^{2+} ion (Figure S2). The S−Zn and O−Zn distances of $Tp^{Ph,Me}Zn$-(ATM) (2.35 and 2.09 Å, respectively) are similar to those in the complex with TM (2.34 and 2.06 Å). In both cases, the oxygen donor atom occupies an axial coordination site, while the sulfur atom is an equatorial donor. The two ligands coordinate the Zn^{2+} with nearly ideal "head-on" binding; the plane formed by the ligand atoms is essentially normal to the plane formed by the three pyrazole nitrogen donors. This angle (ϕ, Figure 2) will be quantified by the torsion angle between
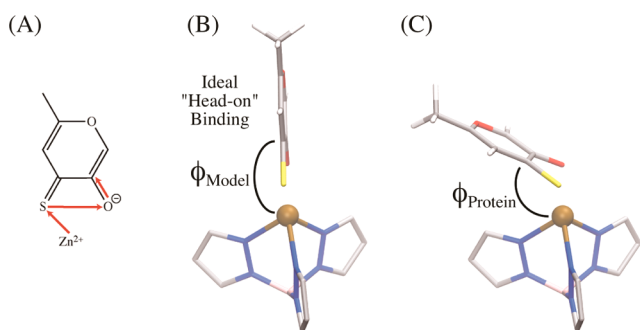

Figure 2. For ATM, TM, and TPMA, ϕ is defined as the Zn^{2+}−S−O-C dihedral angle (A, shown labeled on ATM with red arrows). This parameter defines the angle between the planes formed by the Zn−S−O and S−O−C atoms, representing the tilt of the MBG. MBGs assume different binding modes in $Tp^{Ph,Me}Zn$ (B, ϕ_{Model}) and hCAII (C, $\phi_{Protein}$) complexes. $|\phi_{Model}|$ ranges from 166 to 174°, while $|\phi_{Protein}|$ ranges from 90 to 143° depending on the MBG.

the Zn^{2+} ion, the sulfur donor, the oxygen donor, and the endocyclic carbon bound to the oxygen; these angles show absolute values of 166° and 174° for the $Tp^{Ph,Me}$ complexes of ATM and TM, respectively. Given the similarity of the TM and ATM complexes, it is expected that the TPMA structure would show an identical coordination geometry.

In the active site of hCAII, ATM adopts the expected bidentate coordination mode to the Zn^{2+} ion of hCAII, resulting in trigonal bipyramidal geometry around the metal (Figure 3). The S−Zn (2.57 Å) and O−Zn (2.28 Å) bonds are
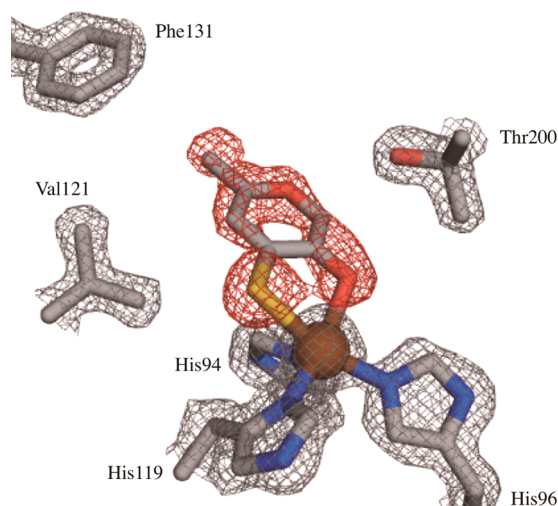

Figure 3. Crystal structure of ATM bound in the active site of hCAII. The $|F_{obs}|$ electron density map (gray) is shown contoured at 1.5σ for protein residues, while the omit $|F_{obs} − F_{calc}|$ map (red) is shown contoured at 3.0σ for ATM. A schematic representation of the interactions between ATM and hCAII can be found in Figure S12.

both ∼0.2 Å longer than those in $Tp^{Ph,Me}Zn$(ATM). As predicted by the model complex, the oxygen donor occupies an axial coordination site, while the sulfur is in an equatorial position. The hydroxyl group of the ligand, in addition to binding the Zn^{2+} ion, is in close proximity to the hydroxyl groups of Thr199 (O−O distance of 3.51 Å) and Thr200 (O−O distance of 3.71 Å), and the methyl group is positioned to interact with the side chains of Val121 and Phe131 of the hydrophobic region of the active site. Due to the steric restrictions of the hCAII active site, the ligand cannot bind in the ideal head-on fashion (ϕ = 180°); it is forced to tilt more than 20° relative to that of the model complex (Figure 2, ϕ = 143°).

The crystal structure of TM bound in the active site of hCAII reveals an unconventional coordination mode: the ligand acts as a monodentate donor through the sulfur atom with a bond length of 2.4 Å, resulting in a distorted tetrahedral geometry around the Zn^{2+} ion. The ligand electron density is best fit as a combination of two binding modes, both with 50% occupancy, in which the coordinated sulfur atoms overlay (Figure 4). In one orientation, the exocyclic hydroxyl and methyl groups are oriented toward the hydrophobic wall of the active site formed by Val143, Leu141, Val121, and Phe131. In the second conformation, the ligand is flipped so that the hydroxyl group is directed toward hydrophilic residues of the active site, allowing for a hydrogen bond with the side chain of Thr200 (O−O distance of 2.85 Å). In this conformation the ring of TM is positioned ∼1.1 Å closer to the to the side chains of Val121 and Val143, allowing for enhanced hydrophobic contacts with these groups. The average B factor of TM is significantly greater than that of ATM (40.5 vs 21.5), consistent with its lower affinity and disordered binding. Efforts to soak TPMA into hCAII crystals repeatedly resulted in poorly defined electron density for the MBG that could not be suitably modeled.
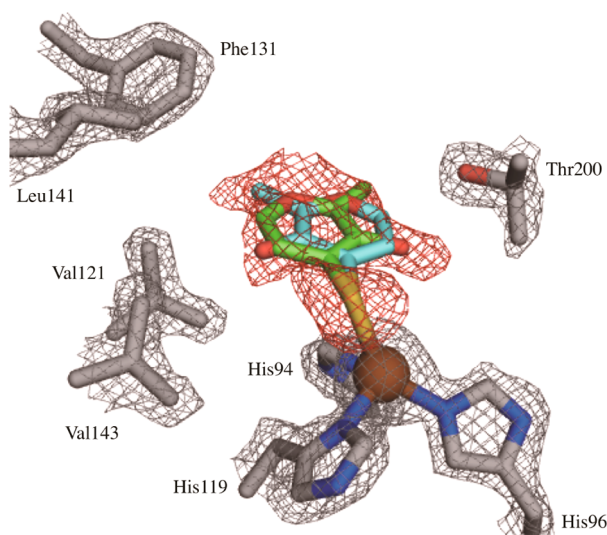
Figure 4. Crystal structure of TM bound in the active site of hCAII. The ligand has two conformations, shown in green and cyan. Omit maps ($|F_{obs}|$, gray; $|F_{obs} - F_{calc}|$, red) are shown contoured at 1.5σ. A diagram of the interactions between THM and hCAII can be found in Figure S12.

X-ray Absorption Spectroscopy. X-ray absorption spectroscopy (XAS) data suggest the binding modes observed in the crystal structures are representative of those present in frozen solution. The data for hCAII with and without the MBGs (ATM, TM, and TPMA) are shown in Figure 5.
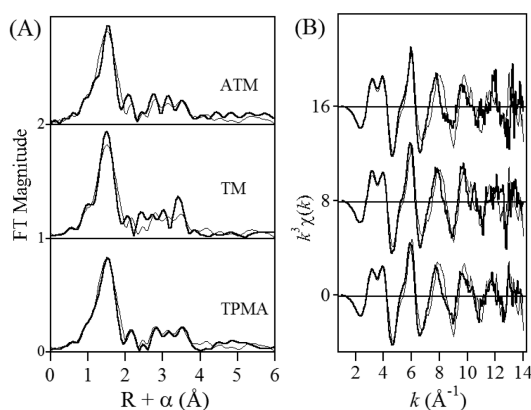

Figure 5. Fourier transforms (A) of the k^3-weighted EXAFS (B) of hCAII with ATM, TM, and TPMA. In each case, the data for the resting enzyme are shown as a thin line overlay.

Detailed fitting results for each data set are given in Figures S3−S6 and Tables S3−S6. Comparison of the Fourier transforms (FTs) in Figure 5A shows that each MBG (bold lines) leads to only minor overall perturbations relative to the resting enzyme (thin lines). ATM provides the most striking changes in the first shell, with both a shift to higher R and narrowing of the main peak (chiefly Zn−N/O scattering), together with increased amplitude at $R + \alpha \sim 2.1$ Å (chiefly Zn−S). The TM complex shows similar, although more subtle, changes in the first shell scattering and substantial changes in the outer shell scattering pattern. The TPMA complex is most similar to the resting enzyme, with only subtle changes in the first shell apparent in the extended X-ray absorption fine structure (EXAFS) FTs. However, examination of the k-space

EXAFS data (Figure 5B) reveals that all three MBGs cause a similar shift in the third oscillation of the EXAFS ($k \sim 7 - 9$ Å^{-1}). Comparison of the theoretical EXAFS for Zn−N and Zn−S interactions shows this is where the two patterns are most likely to show visible divergence (Figure S7), suggesting that all three MBG complexes include a Zn−S scattering interaction. Each MBG causes a similar shift in the shape of the Zn X-ray absorption near edge structure (XANES, Figure S8), also consistent with S-coordination.

The curve fits are consistent with the qualitative assessment given above. The ATM complex with hCAII appears 5-coordinate, with the sulfur of the MBG directly coordinated (fits that excluded the Zn−S bond gave fit residuals that were 3-fold larger, Figure S4 and Table S4). The Zn−N/O distance is also slightly longer than for the resting enzyme and the other two MBG complexes, suggesting higher coordination in the ATM complex, and it is this XANES spectrum that shows that largest energy shift. In contrast, fits to the TM complex data suggest that the total coordination number remains at four with the MBG coordinated through only the sulfur atom (fits that excluded the Zn−S bond gave fit residuals that were 2- to 3-fold larger, Figure S5 and Table S5). This is consistent with the change in the outer shells, where more linear MBG coordination could potentially amplify multiple-scattering interactions, although a deeper analysis is outside the scope of the present study. TM also produces a change in shape in the XANES but a smaller energy shift than ATM. The TPMA complex is strikingly similar to the resting enzyme with only the shift in principal frequency noted above being readily apparent. Fits to these data also suggest retention of a total coordination of four in the TPMA complex (as observed for TM), with the MBG S-bound (fits that excluded the Zn−S bond gave fit residuals that were approximately 2-fold larger, Figure S6 and Table S6). This is supported by the XANES, which clearly show a change in shape on addition of TPMA.

Computational Analysis. To assess one possible cause for the switch to monodentate coordination of TM and TPMA in the active site of hCAII, linear transit computations employing density functional theory (DFT) were conducted along ϕ from 180° to 90° for TM complexed to the simplified TpZn scaffold. Near $\phi = 180°$, the plane formed by TM is perpendicular to the plane defined by the three Zn^{2+}-coordinating pyrazole nitrogens. Similar to the Tp^{Ph,Me}Zn(TM) crystal structure, this computed structure adopts a trigonal bipyramidal geometry with the hydroxyl group as an axial donor and the sulfur donor coordinating equatorially. The calculated O−Zn and S−Zn distances (2.08 and 2.45 Å, respectively) are similar to those observed in the crystal structure of Tp^{Ph,Me}Zn(TM) (Figure S9).

As TM is tilted along ϕ, the Zn donor atom distances increase gradually until ϕ reaches 120°, which is the last point along the linear transit where the ligand coordination is bidentate (Figure 6). For values of $\phi < 120°$, no stationary states corresponding to bidentate coordination of the Zn^{2+} ion are obtained; monodentate coordination by the thione becomes the favored binding mode. At these points, the O−Zn distance is >3.4 Å, while the S−Zn bond length, having a value of 2.30 − 2.32 Å, more closely resembles a thiolate−Zn^{2+} bond.[38] Similar trends in coordination mode along the ϕ reaction coordinate are also present for TM and TPMA (Figure 6).

For all three MBGs, the lowest energies are achieved at values of ϕ near 180°, where the ligand assumes its ideal "head-on" binding mode as observed in the model complexes.
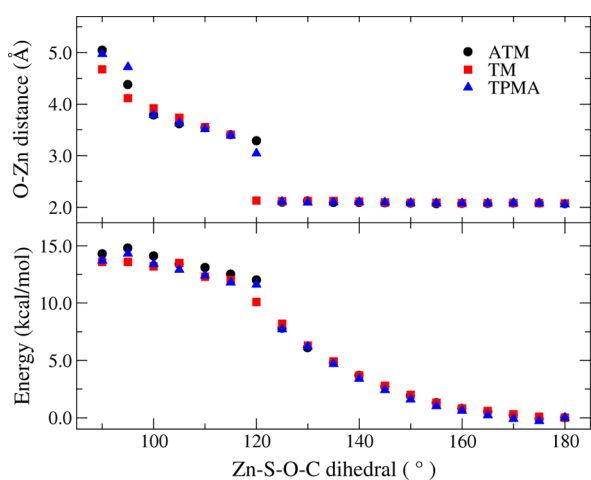
Figure 6. Calculated O–Zn distances (top) and relative binding energies (bottom) as a function of ϕ from linear transit computations.

Distorting the ligand coordination from $\phi = 180°$ leads to an increase in energy relative to the head-on binding geometry, and the energy of the complex appears to follow a parabolic path up to the point where the coordination mode shifts from bidentate to monodentate (Figure 6). Shifting to monodentate coordination of Zn^{2+} through the sulfur atom causes the relative energy of the complex to level out at ~12−15 kcal/mol above the energy of the "head-on" binding mode.

■ DISCUSSION

Aside from being tilted away from ideal "head-on" binding, the coordination of ATM to the active site Zn^{2+} ion of hCAII is similar to that predicted by the $Tp^{Ph,Me}$ model complex (Figure S2). This bidentate coordination mode has been previously reported for 2-mercaptopyridine-N-oxide (1,2-HOPTO), a similar MBG (Figure 7).[39] The previously reported K_i of 1,2-
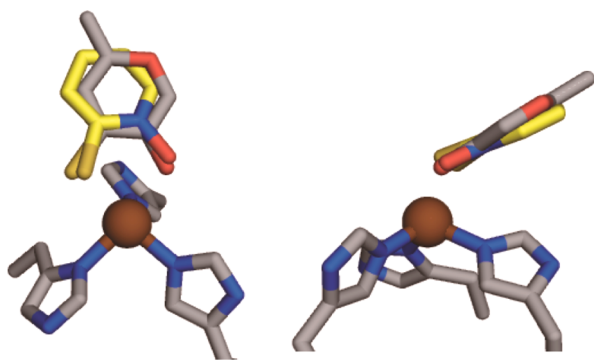

Figure 7. Overlay of the crystal structures of ATM and 1,2-HOPTO (PDB ID 3M1K, shown in yellow) bound to hCAII. Although the donor atoms are positioned similarly (left), a view along the plane of the ligands (right) reveals that ATM is ~10° closer to ideal "head-on" binding.

HOPTO against hCAII (0.85 mM) is close to that of ATM and coincides with the similar binding mode.[3] Although the interaction between ATM and the Zn^{2+} ion appears to be bidentate, the residual inhibitory activity of ATM-OMe suggests that the electrostatic interaction between the oxygen donor and the Zn^{2+} ion is not essential for binding.

The coordination mode of TM to the active site Zn^{2+} ion of hCAII demonstrates that a protein environment can strongly

perturb MBG coordination. The inhibitory activity of ATM-OMe suggests that the interaction between the hydroxyl group and the Zn^{2+} ion is not essential for activity, and the monodentate binding of TM further supports this. While the methyl group of ATM is ideally positioned for hydrophobic interactions when the ligand adopts bidentate coordination, this is not the case for TM. It appears that in order to maximize other protein−ligand interactions, the O−Zn binding interaction is sacrificed. The conformation in which the hydroxyl and methyl groups are oriented toward the hydrophobic wall of the active site is very similar to a previously reported structure of 2-mercaptophenol (2-MP) bound to hCAII (Figure 8).[40]
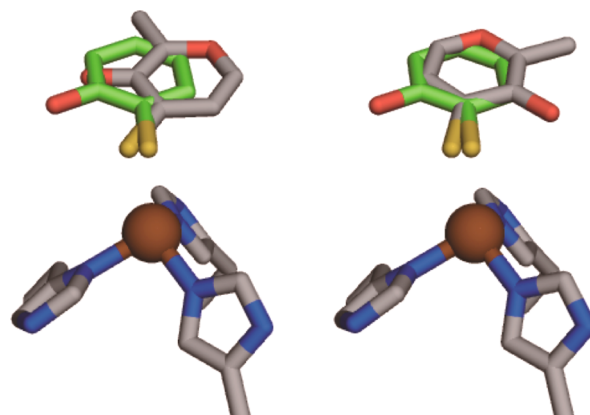

Figure 8. Overlay of the crystal structure of TM and inhibitors that show similar binding modes. Left: The conformation with the hydroxyl group of TM facing the hydrophobic pocket occupies a space similar to that of 2-mercaptophenol (PDB 2OSM, shown in green). Right: When the hydroxyl group of TM is oriented toward the hydrophilic side of the active site, the ring nearly overlays with that of 2-mercaptophenol.

Although both TM and 2-MP are monodentate ligands in hCAII, only the $Tp^{Ph,Me}$ model complex of 2-MP recapitulates this monodentate binding mode.[41] In contrast, the $Tp^{Ph,Me}$Zn-(TM) complex shows strong bidentate coordination from both the sulfur and oxygen donor atoms. This suggests that while the monodentate binding of 2-MP to hCAII is driven largely by the properties of the ligand itself, the monodentate binding mode of TM is a direct result of interactions with the hCAII active site environment.

In contrast to TM, which loses all inhibitory activity when methylated (TM-OMe), when the hydroxyl group of 2-MP is methylated (TG, Figure 1), the activity against hCAII is unaffected (K_i =3.2 ± 0.3 μM for TG vs 3.0 ± 0.7 μM for 2-MP).[3] This suggests that the binding mode of TM that is relevant to inhibition is the conformation in which the hydroxyl and methyl groups are oriented toward the hydrophilic residues of the active site. The loss in potency for TM-OMe is consistent with this binding mode, as the interaction between TM and Thr200 would be diminished and the methoxy group would likely have a steric clash with either neighboring protein residues or well-ordered active site water molecules. With the hydroxyl group oriented toward the hydrophilic side of the pocket, a hypothetical bidentate coordination mode would position the methyl group of TM very close to the hydrophilic side of the active site, where well-ordered water molecules interact with protein residues. Consequently, TM rotates toward a monodentate coordination of Zn^{2+} to preserve the preexisting interactions in the pocket. The microscopic pK_a

values of TM in the active site of hCAII are computed to be 4.1 and 7.2 when the hydroxyl group is oriented toward the hydrophilic and hydrophobic pockets, respectively (Figure S11).[42] Coupling these data with the observation of the two conformations in a ~1:1 ratio in the crystal structure determined at pH 8 suggest that at low pH, the predominant species of TM is protonated and oriented toward the hydrophobic pocket (attempts to verify this crystallographically were unsuccessful); at high pH (pH > 7.2), the deprotonated form of TM is dominant with the ligand hydroxyl group oriented in the hydrophilic pocket, which is likely the conformation responsible for the observed inhibitory activity.

From the structural data acquired for TM, particularly when compared to the analogous O,S-donor ATM, it is evident that the Zn^{2+}−MBG interaction is not the sole dictator of ligand binding. Ligand acidity is likely not a major driving force in the change in coordination, as ATM and TM have relatively close acidities (pK_a = 7.64 and 8.06, respectively).[43] The DFT-derived geometric and energetic analyses of TpZn(MBG) complexes show that over the ligand orientations available to MBGs in hCAII ($|\phi|$ = 90−143°), there can be a very small energy difference between monodentate and bidentate coordination of Zn^{2+}. For example, between ϕ = 125−115°, bidentate and monodentate coordination modes for the ligands considered in this study differ in energy by <5 kcal/mol. From this observation, it is reasonable that the orientation of TM can, in some circumstances, be altered by interactions with the active site of hCAII. This finding implies that de novo or fragment-based approaches to inhibitor development must take care to elucidate circumstances where protein effects alter the coordination mode of an MBG.

CONCLUSION

The rational design of metalloprotein inhibitors requires knowledge as to how those inhibitors coordinate the active site metal ion. While small molecule model complexes have been used as proxies for coordination in enzyme active sites, the results presented here demonstrate that the active site environment can have a significant effect on the metal−ligand interaction; in cases where structural data is not available, care must be taken in the assumptions made about metal-inhibitor interaction. In the case of hCAII, the steric restrictions of the active site force ligands to bind in conformations far from ideal head-on binding, drastically decreasing the strength of metal coordination. Other interactions, including hydrogen bonding and hydrophobic contacts, can influence the binding mode of the MBG, leading to coordination modes not observed in conventional coordination chemistry. Studies are underway to further understand the role of metal coordination in the binding of metalloprotein inhibitors and how binding is influenced by other interactions within the active site.

ASSOCIATED CONTENT

$\boldsymbol{S}$ Supporting Information

Full experimental details for ligand synthesis, protein expression and purification, crystal structure collection details and refinement statistics, and complete computational procedures. This material is available free of charge via the Internet at http://pubs.acs.org.

AUTHOR INFORMATION

Corresponding Authors
dtierney@miamioh.edu

scohen@ucsd.edu

Notes

The authors declare no competing financial interest.

REFERENCES

(1) Andreini, C.; Bertini, I.; Cavallaro, G.; Holliday, G. L.; Thornton, J. M. *J. Biol. Inorg. Chem.* **2008**, *13*, 1205−1218.
(2) Supuran, C. T.; Winum, J.-Y. *Drug Design of Zinc-Enzyme Inhibitors*; John Wiley & Sons, Inc.: Hoboken, NJ, 2009.
(3) Martin, D. P.; Hann, Z. S.; Cohen, S. M. *Inorg. Chem.* **2012**, *52*, 12207−12215.
(4) Jacobsen, F. E.; Lewis, J. A.; Cohen, S. M. *ChemMedChem* **2007**, *2*, 152−171.
(5) Kawai, K.; Nagata, N. *Eur. J. Med. Chem.* **2012**, *51*, 271−276.
(6) Jacobsen, J. A.; Fullagar, J. L.; Miller, M. T.; Cohen, S. M. *J. Med. Chem.* **2011**, *54*, 591−602.
(7) Serrao, E.; Odde, S.; Ramkumar, K.; Neamati, N. *Retrovirology* **2009**, *6*, 25.
(8) Saito, A.; Yamashita, T.; Mariko, Y.; Nosaka, Y.; Tsuchiya, K.; Ando, T.; Suzuki, T.; Tsuruo, T.; Nakanishi, O. *Proc. Nat. Acad. Sci. U.S.A.* **1999**, *96*, 4592−4597.
(9) Johns, B. A.; Kawasuji, T.; Weatherhead, J. G.; Taishi, T.; Temelkoff, D. P.; Yoshida, H.; Akiyama, T.; Taoda, Y.; Murai, H.; Kiyama, R.; Fuji, M.; Tanimoto, N.; Jeffrey, J.; Foster, S. A.; Yoshinaga, T.; Seki, T.; Kobayashi, M.; Sato, A.; Johnson, M. N.; Garvey, E. P.; Fujiwara, T. *J. Med. Chem.* **2013**, *56*, 5901−5916.
(10) Looney, A.; Parkin, G.; Alsfasser, R.; Ruf, M.; Vahrenkamp, H. *Angew. Chem., Int. Ed.* **1992**, *31*, 92−93.
(11) Looney, A.; Han, R.; McNeill, K.; Parkin, G. *J. Am. Chem. Soc.* **1993**, *115*, 4690−4697.
(12) Parkin, G. *Chem. Rev.* **2004**, *104*, 699−767.
(13) Puerta, D. T.; Cohen, S. M. *Inorg. Chem.* **2002**, *41*, 5075−5082.
(14) Puerta, D. T.; Schames, J. R.; Henchman, R. H.; McCammon, J. A.; Cohen, S. M. *Angew. Chem., Int. Ed.* **2003**, *42*, 3772−3774.
(15) Puerta, D. T.; Lewis, J. A.; Cohen, S. M. *J. Am. Chem. Soc.* **2004**, *126*, 8388−8389.
(16) Jacobsen, F. E.; Breece, R. M.; Myers, W. K.; Tierney, D. L.; Cohen, S. M. *Inorg. Chem.* **2006**, *45*, 7306−7315.
(17) Cho, J. H.; Kim, D. H.; Chung, S. J.; Ha, N.-C.; Oh, B.-H.; Choi, K. Y. *Bioorg. Med. Chem.* **2002**, *10*, 2015−2022.
(18) Gaucher, J. F.; Selkti, M.; Tiraboschi, G.; Prangé, T.; Roques, B. P.; Tomas, A.; Fournié-Zaluski, M. C. *Biochemistry* **1999**, *38*, 12569−12576.
(19) Supuran, C. T.; Scozzafava, A.; Casini, A. *Med. Res. Rev.* **2003**, *23*, 146−189.
(20) Krishnamurthy, V. M.; Kaufman, G. K.; Urbach, A. R.; Gitlin, I.; Gudiksen, K. L.; Weibel, D. B.; Whitesides, G. M. *Chem. Rev.* **2008**, *108*, 946−1051.

(21) Breiten, B.; Lockett, M. R.; Sherman, W.; Fujita, S.; Al-Sayah, M.; Lange, H.; Bowers, C. M.; Heroux, A.; Krilov, G.; Whitesides, G. M. *J. Am. Chem. Soc.* **2013**, *135*, 15579−15584.

(22) Agrawal, A.; Johnson, S. L.; Jacobsen, J. A.; Miller, M. T.; Chen, L.-H.; Pellecchia, M.; Cohen, S. M. *ChemMedChem* **2010**, *5*, 195−199.

(23) Martin, D. P.; Cohen, S. M. *Chem. Commun.* **2012**, *48*, 5259−5261.

(24) Avvaru, B. S.; Kim, C. U.; Sippel, K. H.; Gruner, S. M.; Agbandje-McKenna, M.; Silverman, D. N.; McKenna, R. *Biochemistry* **2010**, *49*, 249−251.

(25) Murshudov, G. N.; Vagin, A. A.; Dodson, E. J. *Acta Crystallogr.* **1997**, *D53*, 240−255.

(26) Emsley, P.; Cowtan, K. *Acta Crystallogr.* **2004**, *D60*, 2126−2132.

(27) Schüttelkopf, A. W.; Aalten, D. M. F. v. *Acta Crystallogr.* **2004**, *D60*, 1355−1363.

(28) Frisch, M. J.; Trucks, G. W.; Schlegel, H. B.; Scuseria, G. E.; Robb, M. A.; Cheeseman, J. R.; Scalmani, G.; Barone, V.; Mennucci, B.; Petersson, G. A.; Nakatsuji, H.; Caricato, M.; Li, X.; Hratchian, H. P.; Izmaylov, A. F.; Bloino, J.; Zheng, G.; Sonnenberg, J. L.; Hada, M.; Ehara, M.; Toyota, K.; Fukuda, R.; Hasegawa, J.; Ishida, M.; Nakajima, T.; Honda, Y.; Kitao, O.; Nakai, H.; Vreven, T.; Montgomery, J. A., Jr.; Peralta, J. E.; Ogliaro, F.; Bearpark, M.; Heyd, J. J.; Brothers, E.; Kudin, K. N.; Staroverov, V. N.; Kobayashi, R.; Normand, J.; Raghavachari, K.; Rendell, A.; Burant, J. C.; Iyengar, S. S.; Tomasi, J.; Cossi, M.; Rega, N.; Millam, J. M.; Klene, M.; Knox, J. E.; Cross, J. B.; Bakken, V.; Adamo, C.; Jaramillo, J.; Gomperts, R.; Stratmann, R. E.; Yazyev, O.; Austin, A. J.; Cammi, R.; Pomelli, C.; Ochterski, J. W.; Martin, R. L.; Morokuma, K.; Zakrzewski, V. G.; Voth, G. A.; Salvador, P.; Dannenberg, J. J.; Dapprich, S.; Daniels, A. D.; Farkas, Ö.; Foresman, J. B.; Ortiz, J. V.; Cioslowski, J.; Fox, D. J. *Gaussian 09*; Gaussian, Inc.: Wallingford, CT, 2009.

(29) Becke, A. D. *J. Chem. Phys.* **1993**, *98*, 5648−5652.

(30) Lee, C. T.; Yang, W. T.; Parr, R. G. *Phys. Rev. B* **1988**, *37*, 785−789.

(31) Stephens, P. J.; Devlin, F. J.; Chabalowski, C. F.; Frisch, M. J. *J. Phys. Chem.* **1994**, *98*, 11623−11627.

(32) Vosko, S. H.; Wilk, L.; Nusair, M. *Can. J. Phys.* **1980**, *58*, 1200−1211.

(33) Barone, V.; Cossi, M. *J. Phys. Chem. A* **1998**, *102*, 1995−2001.

(34) Cossi, M.; Rega, N.; Scalmani, G.; Barone, V. *J. Comput. Chem.* **2003**, *24*, 669−681.

(35) Klamt, A.; Schuurmann, G. *J. Chem. Soc., Perkin Trans. 2* **1993**, 799−805.

(36) Ryde, U. *Biophys. J.* **1999**, *77*, 2777−2787.

(37) Dudev, T.; Lim, C. *J. Am. Chem. Soc.* **2000**, *122*, 11146−11153.

(38) Rao, C. P.; Dorfman, J. R.; Holm, R. H. *Inorg. Chem.* **1986**, *25*, 428−439.

(39) Wischeler, J. S.; Innocenti, A.; Vullo, D.; Agrawal, A.; Cohen, S. M.; Heine, A.; Supuran, C. T.; Klebe, G. *ChemMedChem* **2010**, *5*, 1609−1615.

(40) Barrese, A. A.; Genis, C.; Fisher, S. Z.; Orwenyo, J. N.; Kumara, M. T.; Dutta, S. K.; Phillips, E.; Kiddle, J. J.; Tu, C.; Silverman, D. N.; Govindasamy, L.; Agbandje-McKenna, M.; McKenna, R.; Tripp, B. C. *Biochemistry* **2008**, *47*, 3174−3184.

(41) Tekeste, T.; Vahrenkamp, H. *Inorg. Chem.* **2006**, *45*, 10799−10806.

(42) Mongan, J.; Case, D. A.; McCammon, J. A. *J. Comput. Chem.* **2004**, *25*, 2038−2048.

(43) Enyedy, É. A.; Dömötör, O.; Varga, E.; Kiss, T.; Trondl, R.; Hartinger, C. G.; Keppler, B. B. *J. Inorg. Biochem.* **2012**, *117*, 189−197.